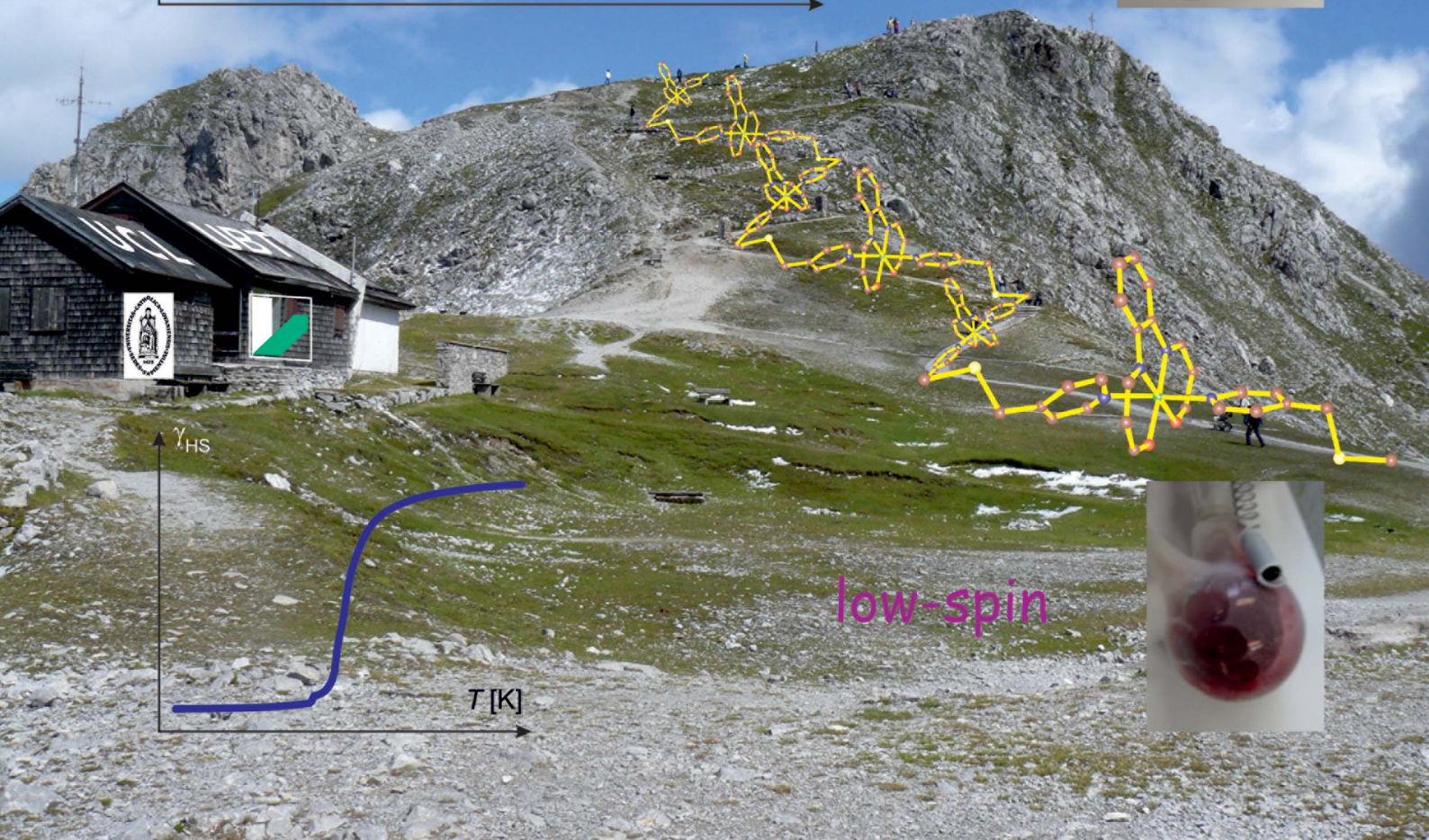


CrystEngComm

www.rsc.org/crystengcomm

Volume 14 | Number 4 | 21 February 2012 | Pages 1167–1492



RSC Publishing

COVER ARTICLE

Weber *et al.*

Iron(II) Spin transition Coordination Polymers with a Zigzag Structure

Cite this: *CrystEngComm*, 2012, **14**, 1223

www.rsc.org/crystengcomm

PAPER

Iron(II) spin transition coordination polymers with a zigzag structure†

Wolfgang Bauer,^a Marinela M. Dîrtu,^b Yann Garcia^{*b} and Birgit Weber^{*a}

Received 22nd September 2011, Accepted 21st November 2011

DOI: 10.1039/c2ce06253d

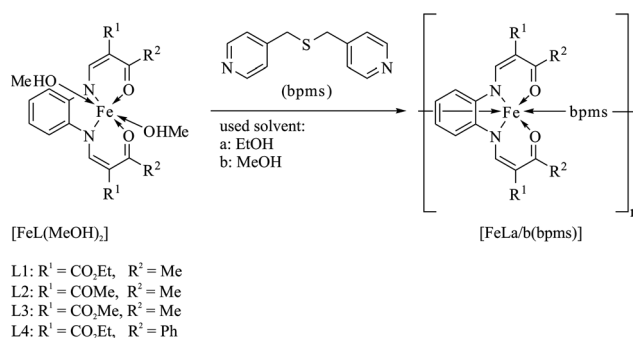
The synthesis and characterisation of seven iron(II) 1D chain coordination polymers with tetradentate Schiff-base like equatorial ligands and bis(4-pyridylmethyl)sulfide (bpms) as a flexible bridging axial ligand is reported. This new family of materials displays a wide spectrum of spin transition properties in the solid state ranging from gradual, abrupt, incomplete to even step-wise that have all been characterized by SQUID magnetometry. The X-ray structure analysis of two complexes at several temperatures is discussed in the frame of their spin crossover properties.

Introduction

The spin crossover (SCO) phenomenon has been receiving an ongoing interest over decades,¹ as various applications in information technology² or as sensors³ and cool channel control units in food and medical storage⁴ can be envisioned. Especially in octahedral iron(II) complexes the spin transition between the paramagnetic high-spin (HS; $S = 2$) and the diamagnetic low-spin (LS; $S = 0$) state is associated with pronounced changes of the physical properties as for example the color, which can be easily detected with the naked eye. Coordinatively bridged networks of SCO complexes have been part of distinctive investigations with the objective to enhance communication between the SCO sites^{2,5} and to control the cooperative interactions.^{1,6,7} Although there is no doubt that the SCO information is propagated in the solid state by strong cooperative interactions transmitted through hydrogen bonding,⁸ π -stacking⁹ or van der Waals-interactions¹⁰ from one molecule to another, many open questions still exist. The occurrence of thermal hysteresis loops and their width in SCO materials as well as the reason for stepped or incomplete spin transitions are not yet fully understood. Looking at 1D coordination polymers we recently confirmed that the SCO behavior is related to the rigidity of the linker molecule, however intermolecular interactions also play a central role in such a way that rigid linkers in combination with additional interaction mechanisms (hydrogen bonds, π -stacking or van der Waals interactions) lead to wide thermal hysteresis.¹¹ Such a behavior can be confirmed by several examples in the

literature,^{12–14} in agreement with an analytical solution of 1D systems which also demonstrates that the width and shape of the hysteresis loop depend on the balance between long and short range interactions.¹⁵ In contrast to this, flexible linkers with pronounced zigzag chain structures often result in stepped or incomplete SCO, depending on intermolecular restraining interactions,¹¹ the occurrence of non-equivalent iron centers¹⁶ or random order–disorder effects of the HS/LS species.¹⁷

In this paper the synthesis and characterization of several 1D chain iron(II) compounds (Scheme 1) with the flexible bridging ligand bis(4-pyridylmethyl)sulfide (bpms) is presented. The aim is to obtain more examples of 1D chain compounds with pronounced zigzag structure and to investigate their spin transition properties. It is important to understand the influence of the mechanical features of the linker (rigid vs. flexible) and the intermolecular interactions (number of short contacts and hydrogen bonds) on the spin transition properties in order to control them in a crystal engineering like approach. The tetradentate Schiff base-like equatorial ligands used in this work are partly well established for the syntheses of a multitude of SCO materials (L1, L2)^{7,18} or promising new derivatives (L3, L4).^{10,19} Through detailed analysis of the magnetic, structural and



Scheme 1 General synthesis of the 1D iron(II) coordination polymers discussed in this work.

^aInorganic Chemistry II, Universität Bayreuth, Universitätsstraße 30, NW 1, 95440 Bayreuth, Germany. E-mail: weber@uni-bayreuth.de; Fax: +49-92155-2157; Tel: +49-92155-2555

^bInstitute of Condensed Matter and Nanosciences, MOST-Inorganic Chemistry, Université Catholique de Louvain, Place L. Pasteur 1, 1348 Louvain-la-Neuve, Belgium. E-mail: yann.garcia@uclouvain; Fax: +32 10472831; Tel: +32 10472826

† Electronic supplementary information (ESI) available. CCDC reference numbers 729769 and 845683–845684. For ESI and crystallographic data in CIF or other electronic format see DOI: 10.1039/c2ce06253d

Table 1 Overview of the compounds discussed in this work and the used abbreviations

LX/solvent	EtOH	MeOH
L1	[FeL1(bpms)] (1a)	[FeL1(bpms)] (1b)
L2	[FeL2(bpms)]·EtOH (2a ·EtOH)	[FeL2(bpms)]·MeOH (2b ·MeOH)
L3	[FeL3(bpms)] (3a)	[FeL3(bpms)]·0.5MeOH (3b ·0.5MeOH)
L4	[FeL4(bpms)] (4a)	[FeL4(bpms)] (4b)

thermodynamic properties of these compounds and comparisons with closely related materials, a relationship between differing intermolecular interactions and the resulting SCO behavior is drawn. In Scheme 1 the general reaction for the synthesis of the complexes is given together with the used abbreviations. An overview of the obtained complexes is given in Table 1. Two classes of complexes can be distinguished, obtained in either ethanol (series **a**) or methanol (series **b**). The complexes are obtained as a black precipitate; thus the color change upon spin transition cannot be followed in the solid. However, in diluted solutions the change is clearly visible as illustrated in ESI, Fig. S1†. The color of the complex strongly depends on the used equatorial ligand.

Results and discussion

Magnetic susceptibility studies

Magnetic susceptibility measurements in the temperature range from 300/350 K down to 10 K were undertaken to follow the iron(II) spin state change for all samples. The thermal dependence of the $\chi_M T$ product (χ_M being the molar susceptibility and T the temperature) for all complexes is displayed in Fig. 1. Of the compounds synthesized with ethanol as a solvent, **1a** and **3a** show a complete and abrupt SCO curve, **4a** shows a complete but gradual SCO behavior and **2a**·EtOH shows a gradual and incomplete SCO behavior, with about three quarters remaining in the HS state. For **1a**, **3a** and **4a** small plateaus at a HS fraction

$\gamma_{HS} \approx 0.1$ are detected. The transition curves of the compounds obtained with methanol as a solvent are quite different from the ethanol samples series, with exception of sample **4b**, which shows an identical transition behavior compared to **4a**. **1b** shows an incomplete gradual spin conversion, **2b**·MeOH is a pure HS complex and the SCO of **3b**·0.5MeOH is complete but also occurs gradually. Thermal hysteresis was observed for none of the samples.

In detail, compounds **1a** and **1b** reach maximum $\chi_M T$ values of 3.24 and 3.08 $\text{cm}^3 \text{K mol}^{-1}$ at 300 K and 350 K, respectively, which is indicative of HS iron(II). Between 300 and 200 K the $\chi_M T$ values for **1a** remain approximately constant. Between 200 and 160 K, the $\chi_M T$ values decrease rapidly, then more gradually, to attain a minimum value of 0.22 $\text{cm}^3 \text{K mol}^{-1}$ ($\gamma_{HS} = 0.07$). The $T_{1/2}^{(1)}$ value of this step is 175 K. Below 160 K, the $\chi_M T$ values further decrease to reach a minimum value of 0.04 $\text{cm}^3 \text{K mol}^{-1}$ at 120 K, indicative of iron(II) in the LS state. The $T_{1/2}^{(2)}$ value of this small step is 157 K. The $\chi_M T$ values of **1b** gradually decrease between 325 and 65 K to attain a minimum value of 1.02 $\text{cm}^3 \text{K mol}^{-1}$ at 65 K, indicating that one-third of the iron(II) sites are still in the HS state. The transition temperature $T_{1/2}$ is 195 K. The differences in the curve progression for **1a** and **1b** can be attributed to the formation of two different polymorphs depending on the used solvent.

The $\chi_M T$ values for **2a**·EtOH remain approximately constant at 3.20 $\text{cm}^3 \text{K mol}^{-1}$ between 300 and 135 K, which is indicative of HS iron(II). Below 135 K the $\chi_M T$ values gradually decrease to reach a minimum value of 2.40 $\text{cm}^3 \text{K mol}^{-1}$ at 60 K, indicating that approximately two-thirds of the iron(II) centers remain in the HS state. The $T_{1/2}$ was evaluated as 89 K, which is very low and agrees well with the transition temperature of another 1D SCO chain [Fe(hyetrz)₃(4-chlorophenylsulfonate)₂·3H₂O (hyetrz = 4,2'-hydroxy-ethyl-1,2,4-triazole).³ **2b**·MeOH remains HS over all temperatures, with a room temperature $\chi_M T$ value of 3.30 $\text{cm}^3 \text{K mol}^{-1}$. The $\chi_M T$ values for **3a** remain approximately constant at 3.30 $\text{cm}^3 \text{K mol}^{-1}$ above 250 K, which confirms that iron(II) ions are in the HS state. Over the range 250–210 K, the $\chi_M T$ values decrease, first rapidly then gradually, to attain a minimum of 0.43 $\text{cm}^3 \text{K mol}^{-1}$ at 210 K ($\gamma_{HS} = 0.13$). The $T_{1/2}^{(1)}$ value of this step is 247 K. Below 210 K the $\chi_M T$ values decrease, again first rapidly then gradually, to attain a minimum value of 0.08 $\text{cm}^3 \text{K mol}^{-1}$ at 175 K. The $T_{1/2}^{(2)}$ value of this little step is 205 K. Below 175 K the $\chi_M T$ values indicate a diamagnetic state. The $\chi_M T$ values for **3b**·0.5MeOH gradually decrease from a maximum of 3.27 $\text{cm}^3 \text{K mol}^{-1}$ at 300 K to a minimum of 0.10 $\text{cm}^3 \text{K mol}^{-1}$ at 50 K. The $T_{1/2}$ derived from this SCO curve is 216 K. Compound **4a** presents a maximum $\chi_M T$ value of 3.34 $\text{cm}^3 \text{K mol}^{-1}$ at 300 K. Below 300 K the $\chi_M T$ values decrease slowly and then more rapidly between 230 and 133 K, and again gradually, to reach a minimum value of 0.35 $\text{cm}^3 \text{K mol}^{-1}$ at 133 K ($\gamma_{HS} = 0.11$). The $T_{1/2}^{(1)}$ value of this step is 179 K. Below 133 K the $\chi_M T$ values drop to 0.06 $\text{cm}^3 \text{K mol}^{-1}$ at 95 K with a $T_{1/2}^{(2)}$ of 125 K for this small step. The thermal spin transition behavior of compound **4b** does not differ from that observed for **4a**. Since complex **1a** displays a sharp spin state transition, it was investigated in more detail by recording once again magnetic data with a very slow cooling rate (1 K min⁻¹), the result of which is shown in Fig. 2. A careful analysis of the magnetic data reveals that the spin transition proceeds in three steps with two anomalies at

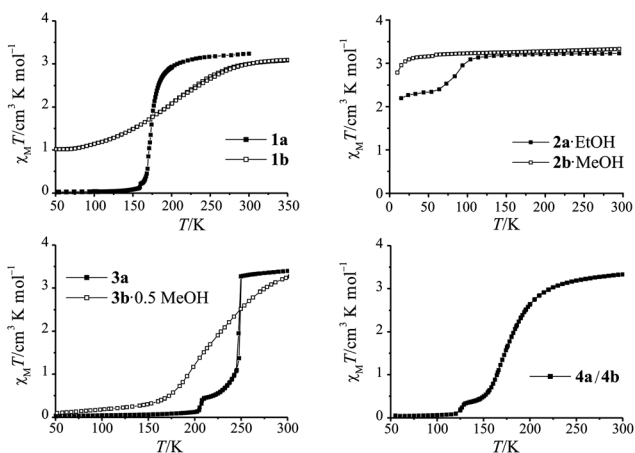


Fig. 1 Plots of the $\chi_M T$ product vs. T over the range 50–300 K (350 K) for the compounds discussed in this work and the solvents used for synthesis (filled squares: ethanol, open squares: methanol).

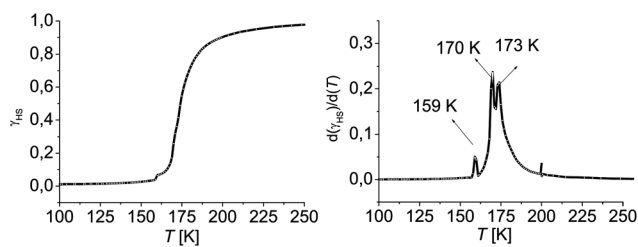


Fig. 2 HS molar fraction γ_{HS} derived from magnetic data of **1a** recorded at 1 K min^{-1} over the range 50–300 K. The right figure shows the first derivative of the HS molar fraction.

~ 172 K and ~ 159 K. This assumption is confirmed by looking at the first derivative of the HS molar fraction, γ_{HS} , derived from magnetic data, with the detection of two maxima at 170 K and 173 K. A tiny step is also observed at 159 K, which was also seen in the first magnetic measurement (Fig. 1a).

Differential scanning calorimetry

Intrigued by the three step nature of the ST process in **1a**, we undertook a differential scanning calorimetry (DSC) study over the temperature range 300–98 K on cooling and warming modes, at 10 K min^{-1} . On cooling from room temperature, two exothermic peaks are observed at 176(1) K and 172(1) K, which correspond to a first order phase transition proceeding in two steps (Fig. 3). On warming, the phenomenon is reversible with two endothermic peaks observed at 174(1) K and 177(1) K. These data match well the anomalies detected in the SQUID measurements at 170 K and 173 K with the differences in scanning velocity to be taken into account (see Fig. 2). The magnetic anomaly found at 159 K is not observed by DSC. The same thermal profile was obtained after having cycled the sample several times. The thermodynamic parameters were evaluated as $\Delta H = 5(1)$ kJ mol^{-1} and $\Delta S = 28.9(1)$ J mol^{-1} K^{-1} .

X-Ray structure analysis

Crystals suitable for X-ray analysis of compounds **1a** and **4b** were obtained by a slow diffusion technique. The crystallographic data are summarised in Table 5. Fig. 4 and 5 display the asymmetric units of **1a** and **4b**, respectively. Selected bond lengths and

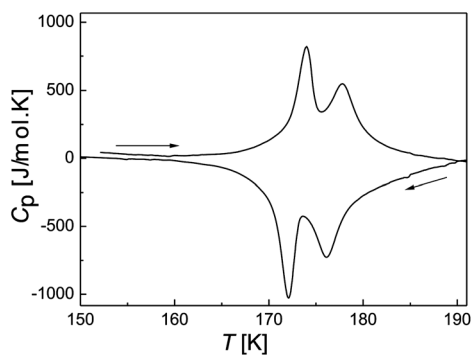


Fig. 3 Heat capacity vs. T of **1a** recorded over the temperature range 300–98 K at a scanning rate of 10 K min^{-1} in the cooling (\leftarrow) and warming (\rightarrow) modes.

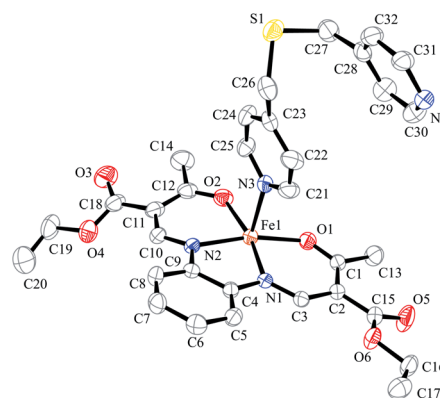


Fig. 4 ORTEP drawing of the asymmetric unit of **1a**. Hydrogen atoms were omitted for clarity. Thermal ellipsoids are shown at the 50% probability level.

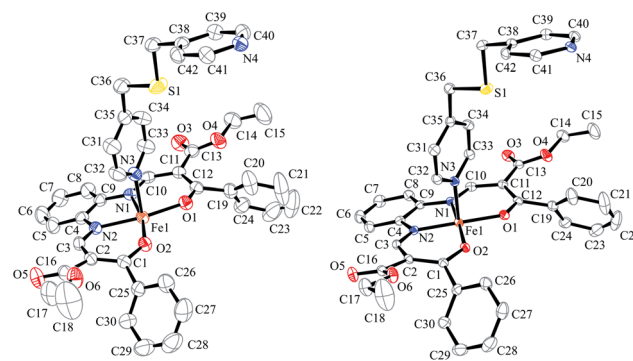


Fig. 5 ORTEP drawing of the asymmetric unit of **4b^{HS}** at 250 K (left) and **4b^{LS}** at 125 K (right). Hydrogen atoms were omitted for clarity. Thermal ellipsoids are shown at the 50% probability level.

angles around the inner coordination sphere of the iron centres are summarised in Table 2. The determination of the X-ray structure of **1a** in the LS state was not possible, as the crystals crumble while cooling, despite a slow cooling rate of 2 K min^{-1} . For compound **4b** it was possible to determine the crystal structure in the HS (**4b^{HS}**) and LS state (**4b^{LS}**), which is very important to get a deeper insight into the observed SCO behaviour.

Both complexes have in common the fact that the iron(II) centres are located in an octahedral coordination sphere consisting of the equatorially coordinated tetradentate Schiff base-like ligand and the axially coordinated bis-monodentate bridging ligand bpms, bound through terminal 4-pyridyl groups. Each bridging ligand “connects” two iron(II) centres, resulting in the formation of infinite 1D chains as given in Fig. 6. Due to the “flexibility” of the axial ligand with its sulfide bridge, the 1D chains of both compounds propagate in a zigzag-like manner. Compound **1a^{HS}** crystallises in the monoclinic space group $P2_1/c$, with four formula units in the unit cell.

The observed bond lengths around the iron(II) centre of **1a^{HS}** are within the range reported for other octahedral iron(II) complexes of this ligand type in the HS state.^{7,11} The average values are 2.08 Å (Fe– N_{eq}), 2.01 Å (Fe– O_{eq}) and 2.27 Å (Fe– L_{ax}). The observed O–Fe–O angle, the so-called bite angle of the ligand, which is typically about 110° for HS iron(II) complexes of

Table 2 Selected bond lengths [Å] and angles [degree] within the inner coordination sphere of the iron(II) coordination polymers discussed in this work

	Fe1–N1/2	Fe1–O1/2	Fe1–L _{ax}	O1–Fe1–O2	L _{ax} –Fe1–L _{ax}
1a	2.083(2) 2.083(2)	1.994(2) 2.016(2)	2.242(3) 2.296(3) ^a	107.33(8)	179.19(9) ^a
4b^{HS}	2.0823(15) 2.0757(15)	1.9965(12) 2.0069(12)	2.2296(16) 2.2362(15) ^b	105.16(5)	177.65(6) ^b
4b^{LS}	1.9165(15) 1.9133(15)	1.9418(13) 1.9536(11)	2.0115(15) 2.0226(14) ^b	90.56(5)	176.81(6) ^b

^a $1 + x, 1/2 - y, 1/2 + z$. ^b $x, 1/2 - y, -1/2 + z$.

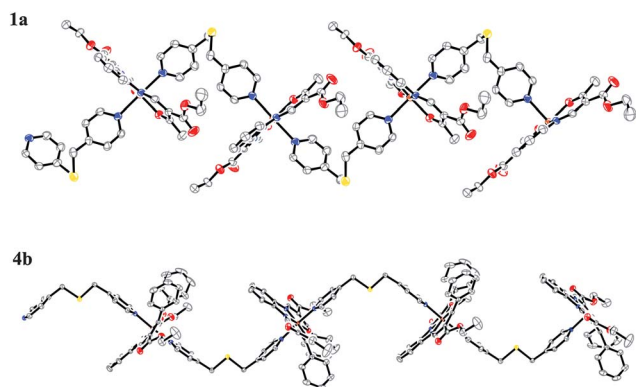


Fig. 6 Top: excerpt of the 1D chain of compound **1a** in the crystal. The zigzag motif is due to the twisted bridging ligand. Bottom: excerpt of the zigzag 1D chain of compound **4b** in the crystal (using the example of **4b^{LS}**). Hydrogen atoms were omitted for clarity.

this ligand type and about 90° for LS iron(II), is with 107.3° clearly indicative of iron(II) in the HS state. The parallel 1D chains of **1a^{HS}** propagate along the [2 0 1] direction and are stacked such that the unit cell contains no residual solvent accessible void volume. The intra-chain Fe1...Fe1 separation distance is with 10.02 Å rather short, highlighting the strong twisting of the axial bpms ligand (Fig. 6) and the close-packed nature of the chains of **1a^{HS}** (Fig. 7). Such a packing motif was also found in the crystal structure of the closely related compound [FeL1(bppa)]¹¹ (bppa = 1,3-bis(4-pyridyl)propane, Fe1...Fe1 = 10.01 Å), which undergoes an incomplete SCO that stops at an intermediate plateau of the 50% HS-fraction.

Compounds **4b^{HS}** and **4b^{LS}** crystallise in orthorhombic space group *Pbca*, with eight formula units in the unit cell. The average bond lengths within the first coordination sphere of the iron(II) centres in the HS-structure are 2.08 Å (Fe–N_{eq}), 2.00 Å (Fe–O_{eq}) and 2.23 Å (Fe–L_{ax}). The observed O–Fe–O angle is with 105.2° at the lower limit of the expected HS-values of this ligand type,^{7,11} indicative of a beginning spin transition at slightly lower temperatures. Upon spin transition a shortening of the bond lengths of about 10% is observed, as discussed for other iron(II) spin crossover complexes in the literature.¹ The average bond lengths in the LS-structure are with 1.92 Å (Fe–N_{eq}), 1.95 Å (Fe–O_{eq}) and 2.01 Å (Fe–L_{ax}) in the typical range for an octahedral iron(II) LS centre. The more pronounced bond shortening of the axial ligand, which connects the iron centres in the 1D chain, is in agreement with previous findings on mononuclear

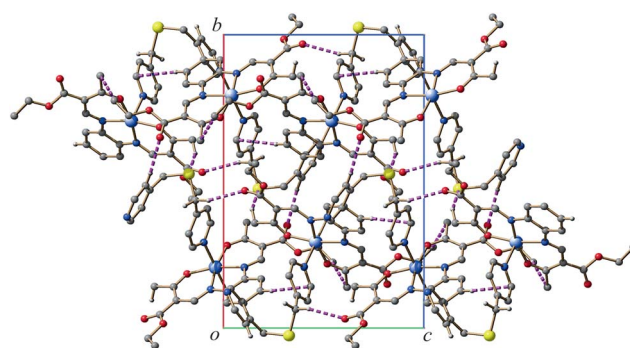


Fig. 7 Molecule packing of compound **1a** in the crystal. View along [1 0 0].

analogues.^{7,18} The observed value of the O–Fe–O angle is with 90.6° clearly indicative of LS iron(II). Together with the bond shortening the cell volume shrinks from 8055.4(6) to 7675.7(6) Å³, comparing the HS- with the LS-structure. Considering the additional contribution of the thermal cell contraction, the observed change of the cell volume $\Delta V/V = 4.7\%$, $\Delta V = 47.5$ Å³ per Fe, is in the range expected for an iron(II) SCO complex (sole contribution of the SCO: $\Delta V/V = 3.8\text{--}6\%$; $\Delta V = 25\text{--}35$ Å³ per Fe)¹ with no indications of strong cooperative effects.

The parallel 1D chains of **4b^{HS}** and **4b^{LS}** propagate along the [0 0 1] direction. They are stacked such that there is a total potential solvent accessible void volume of 621.6 and 466.5 Å³, respectively, which is hypothetically enough space for small molecules like toluene. As can be seen from the molecule packing in Fig. 9, the porosity results from the arrangement of the chains such that the iron centres together with the equatorial ligands and the axial ligands alternately form layers perpendicular to the [0 0 1] direction. In contrast to **1a**, the axial bridging ligand is not twisted. In line with this finding are the observed intra-chain Fe1...Fe1 separation distances of 12.89 and 12.69 Å for **4b^{HS}** and **4b^{LS}**, respectively, which attests to a straight-lined structure of the axial ligand.

Intermolecular interactions

The investigation of intermolecular interactions is of great significance for an understanding of the magnetic properties. In Tables 3 and 4 short intermolecular contacts of the complexes discussed in this work are summarised. In Fig. 7–9 excerpts of the molecule packing of the complexes are shown. Due to the close packing of **1a^{HS}** numerous short interchain contacts in the form of non-classical hydrogen bonds can be found (Fig. 7). The strongest interactions can be observed between the hydrogen atoms H26 and H32 belonging to the CH₂ group and the pyridine ring of the axial bpms ligand and the carbonyl oxygen atoms O5 and O3 located at different equatorial ligands of adjacent chains, overall building up a 3D network of short contacts.

Moreover the sulfur atom acts as an acceptor of hydrogen atom H13B of the methyl group of the equatorial ligand. In comparison to **1a^{HS}**, the HS-structure of the related compound [FeL1(bppa)]¹¹ provides a higher number of intermolecular interactions. Structure analysis at the intermediate plateau revealed that the relocation of the bridging ligands towards the smaller LS iron(II) centre could not follow the Fe–L bond decrease, generally observed for a HS–LS transition.^{7a,20} In

Table 3 Analysis of short intermolecular contacts [\AA] less than the sum of the van der Waals radii, $d(I - J) < R(I) + R(J)$, of **1a**

I	J	$d(I - J)$	$R(I) + R(J)$	Δ
H26	O5 ^a	2.45	2.72	-0.27
H32	O3 ^b	2.54	2.72	-0.18
H20C	C14 ^a	2.76	2.90	-0.14
H13B	S1 ^c	2.94	3.00	-0.06
H7	C25 ^a	2.86	2.90	-0.04
H14A	H20 ^a	2.37	2.40	-0.03

^a $x, 1/2 - y, 1/2 + z$. ^b $2 - x, -y, 1 - z$. ^c $2 - x, 1/2 + y, 1/2 - z$.

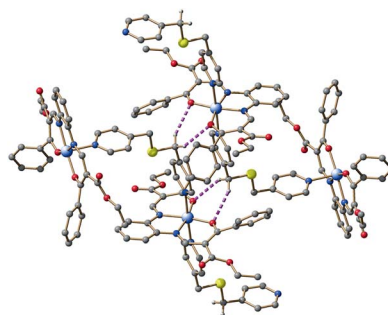
Table 4 Analysis of short intermolecular contacts [\AA] less than the sum of the van der Waals radii, $d(I - J) < R(I) + R(J)$, of **4b^{HS}** and **4b^{LS}**

	I	J	$d(I - J)$	$R(I) + R(J)$	Δ
4b^{HS}	H37B	O1 ^a	2.58	2.72	-0.14
	H37A	O2 ^a	2.60	2.72	-0.12
	H40	O5 ^b	2.60	2.72	-0.12
4b^{LS}	H40	O5 ^b	2.51	2.72	-0.21
	H37A	O2 ^a	2.55	2.72	-0.17
	H37B	O1 ^a	2.56	2.72	-0.16
	H37A	C26 ^a	2.80	2.90	-0.10
	H41	O3 ^c	2.63	2.72	-0.09
	H36A	C20 ^a	2.84	2.90	-0.06
	H37B	C19 ^a	2.85	2.90	-0.05
	H17A	C8 ^d	2.85	2.90	-0.05
	H23	O3 ^e	2.67	2.72	-0.05
	H21	C27 ^b	2.87	2.90	-0.03

^a $-x, -1/2 + y, 1/2 - z$. ^b $-1/2 + x, y, 1/2 - z$. ^c $1/2 + x, y, 1/2 - z$. ^d $1/2 + x, 1/2 - y, -z$. ^e $-1/2 - x, 1/2 + y, z$.

contrast, every second Fe...Fe distance along a chain was even increased. If the number of intermolecular interactions is related to the strength of restraining interactions for the ligand relocation upon SCO, when talking about twisted zigzag structures, this would explain the different SCO behaviour of the two compounds.

The interchain contacts of the HS-structure **4b^{HS}** are less numerous compared to **1a^{HS}** and overall only a 2D network of interactions can be observed, which is spread through the layers build-up of equatorial ligands. This nicely explains the more gradual SCO of compound **4b**. Two non-classical hydrogen bonds involving the iron-coordinating oxygen atoms O1 and O2 of the equatorial ligand and the hydrogen atoms H37A and H37B of a secondary CH₂ group located at the axial ligand of an adjacent chain can be seen as structure-bearing, as they obviously define the straight-lined arrangement of the chains (Fig. 8). Moreover, the carbonyl oxygen O5 acts as an acceptor for hydrogen H40 belonging to a CH group of a pyridyl ring. When going from **4b^{HS}** to the LS-structure **4b^{LS}**, the number of short intermolecular contacts increases, but the additionally found contacts, besides the interactions already characterised at **4b^{HS}**, only facilitate the 2D network mentioned above (Fig. 9). The closely related compound [FeL4(bppa)]·0.5MeOH¹⁰ we recently investigated provides a very similar structure motif: this compound undergoes an incomplete spin transition that rests at an intermediate plateau at the 50% HS-fraction and shows a 5 K wide thermal hysteresis loop. Other than for **4b**, a 3D network of intermolecular contacts could be observed already for the

**Fig. 8** Illustration of structure-bearing interchain contacts of **4b**, using the example of **4b^{HS}**. Intermolecular interactions less than the sum of the van der Waals radii are depicted in dashed bonds. Hydrogen atoms which do not participate in short contacts have been omitted for clarity.

HS-structure of [FeL4(bppa)]·0.5MeOH,¹⁰ which increases the total communication of elastic interactions. The stabilisation of the mixed HS/LS state through the whole low-temperature range was mainly explained by π -stacking of the 1,2-disubstituted benzene rings of the equatorial ligand of two adjacent chains and the upcoming restraining interaction for the ligand relocation. This effect is significantly weaker for **4b^{HS}** than for the HS-structure of [FeL4(bppa)]·0.5MeOH ($C \cdots C = 3.55 \text{ \AA}$ compared to 3.43 \AA).

Discussion

We recently established a correlation between the cooperative effects of some monomeric, dimeric and 1D polymeric coordination SCO compounds and their structural properties derived from X-ray structure analysis, the so-called crystal contact index, CCI,¹⁰ that is the sum of all short and weighted contacts. We assumed that every short contact (shorter than the sum of the van der Waals radii) contributes to the interactions mediating the cooperative effect. Those which are very short contribute more to the cooperative effect than those which are longer. This correlation nicely explains up to small hysteresis loops with the model of elastic interactions. It provides a good estimation to accompany the structural interpretation of spin transition properties. The CCI of compound **1a^{HS}** of 0.31 is relatively small, indicating that low cooperativity can be expected which is in line with results of the magnetic measurement, as thermal hysteresis was not observed. For compound **4b^{HS}** the CCI value is 0.14 which is even lower, which is in line with the presumption that the 2D network of intermolecular contacts is responsible for the more gradual SCO behaviour in contrast to the abrupt spin transition of compound **1a^{HS}**. Upon cooling the CCI value increases to 0.36 (**4b^{LS}**) indicating that the number of short contacts has increased. For the two very similar complexes with bppa as the axial ligand, step-wise spin transitions were observed in both cases.^{10,11} For [FeL4(bppa)]·0.5MeOH,¹⁰ the observed CCI of 2.0 is significantly higher than for **4b**. This correlates well with the observed small hysteresis loop in the case of [FeL4(bppa)]·0.5MeOH¹⁰ and the absence of any cooperative interactions for **4b**. The second pronounced difference between the two spin transition curves is the complete, one-step spin transition of **4b** and the incomplete spin transition of [FeL4(bppa)]·0.5MeOH¹⁰ that stops at the intermediate plateau ($\gamma_{\text{HS}} = 0.5$). According to our model,¹¹

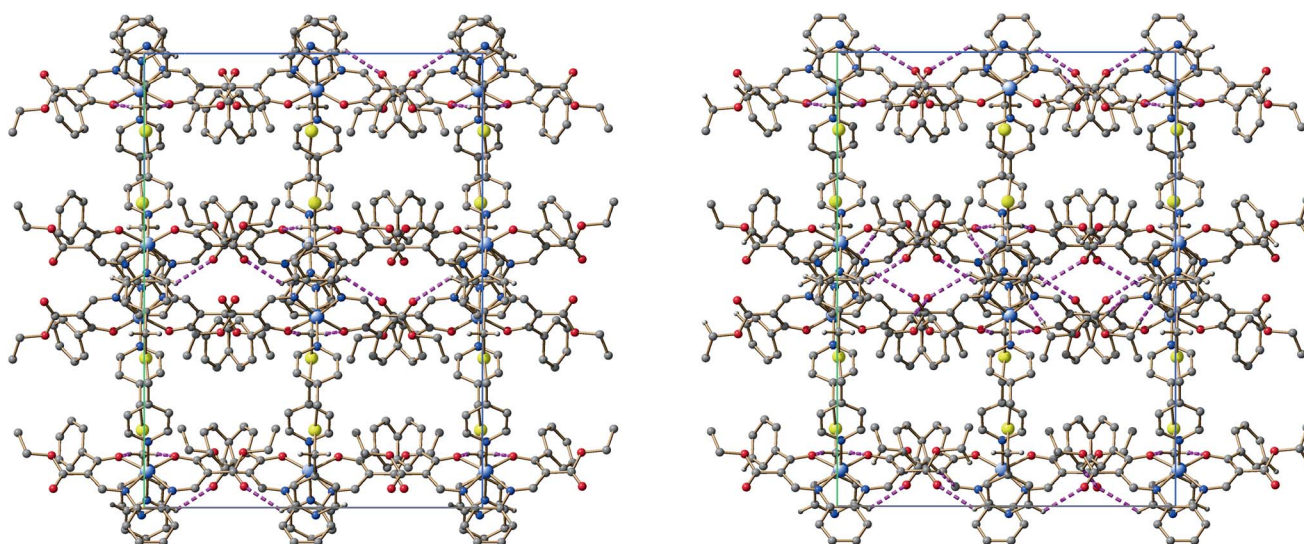


Fig. 9 Left: molecule packing of compound $4a^{HS}$ in the crystal at 250 K. Right: molecule packing of compound $4a^{LS}$ in the crystal at 125 K. View along $[0\ 1\ 0]$ (a -axis: grey, c -axis: green). Intermolecular interactions less than the sum of the van der Waals radii (dashed bonds) can be only observed within layers formed by equatorial ligands. Hydrogen atoms which do not participate in short contacts have been omitted for clarity. The porous structure created by straight-lined arrangement of the 1D chain.

restraining interactions between adjacent chains are responsible for the occurrence of steps during the spin transition of 1D chain compounds (if there are no other reasons as non-equivalent iron centres). Obviously the strength of those interactions also correlates with the number and strength of intermolecular contacts that is reflected in the CCI. This is confirmed if the pair **1a** and $[\text{FeL1}(\text{bppa})]$ is also taken into account. For **1a** the CCI is higher compared to **4b** and consequently the spin transition is more abrupt. Additionally, the very slow measurement mode in the SQUID reveals two different steps in the transition curve—an observation that is confirmed by differential scanning calorimetry (Fig. 3). The higher CCI also reflects higher restraining interactions between the neighbouring zigzag chains. For $[\text{FeL1}(\text{bppa})]^{11}$ a similar transition curve as for $[\text{FeL4}(\text{bppa})] \cdot 0.5\text{MeOH}^{10}$ is observed. The very abrupt and incomplete (IP at $\gamma_{HS} = 0.5$) character correlates well with the higher number of intermolecular contacts. These results show that a purposeful synthesis of SCO compounds with steps in the transition curve is possible. In order to achieve such a rare magnetic behaviour, flexible bridging ligands that lead to pronounced zigzag chains in combination with several interchain interactions are necessary. This example thus demonstrates how useful crystal engineering concepts can be to the design of SCO materials.²¹

The nature of the small step observed in some of the transition curves (**1a**, **3a** and **4a/b**) remains intriguing. Whereas it cannot be attributed to an impurity as all measurements were carried out on crystalline materials, this phenomenon seems not to involve enough entropy to be detected by differential scanning calorimetry. Further investigations, *e.g.* by ^{57}Fe Mössbauer spectroscopy, may be useful to clarify this unusual behaviour.

Conclusions

The combination of four different tetradentate equatorial ligands LX (with $X = \text{L1, L2, L3, L4}$) with bpms as the bridging axial

ligand and methanol or ethanol as the solvent led to a series of 1D chain iron(II) compounds of the general formula $[\text{FeLX}(\text{bpms})] \cdot \text{solvent}$, whose synthesis and characterisation is described in this paper. Structural analyses of **1a**^{HS} and **4b**^{HS/4b}^{LS} reveal zigzag chain structures for both compounds that were expected due to the high similarity between the bppa and the bpms ligands. The magnetic measurements reveal gradual, abrupt and incomplete spin transition curves, however there is no pronounced plateau formation as observed for the complexes with bppa as the axial ligand. This is in line with the lower CCI values of the two complexes with bpms, indicating weaker cooperative effects within the crystal. Obviously, a 1D zigzag chain is not solely responsible for the step formation but restraining interchain interactions are also necessary. These results confirm our models for the explanation of steps and hysteresis in 1D chain iron(II) SCO complexes.

Experimental

Synthesis

All syntheses were carried out under $\text{Ar}_{(g)}$ using Schlenk tube techniques. All solvents were purified as described in the literature and distilled under argon.²² The syntheses of the methanol containing complexes $[\text{FeLX}(\text{MeOH})_2]$ (with $X = 1,^{23} 2,^{22} 3,^{19b} 4,^{24}$ Scheme 1) and anhydrous iron(II) acetate²⁵ as starting material were described. 4-(Chloromethyl)pyridine hydrochloride and sodium sulfide hydrate (65%) were purchased from Fluka and Acros Organics, respectively, and used as received.

Bis(4-pyridylmethyl)sulfide (bpms). To a solution of 4-(chloromethyl)pyridine hydrochloride (4.00 g, 24.4 mmol) and sodium hydroxide (0.98 g, 24.4 mmol) in water (45 mL) was slowly added a solution of sodium sulfide hydrate (1.46 g, 12.2 mmol) in water (30 mL). The resulting dark red mixture was heated to 80 °C for 2

h and then stirred at room temperature for 24 h. Afterwards the reaction mixture was extracted several times with diethyl ether and the combined organic phases were dried over MgSO₄. Removal of the solvent left the product as a red oily residue which was solidified at -26 °C (yield: 1.61 g, 61%). ¹H NMR (400 MHz, CDCl₃, 25 °C, TMS): δ = 8.57–8.60 (m, 4H, Ar–NCH), 7.28–7.31 (m, 4H, Ar–CH), 3.59 ppm (s, 4H; CH₂); MS (DEI(+), 70 eV): *m/z* (%): 216 (84) [M⁺], 124 (45) [C₆H₆NS⁺], 93 (100) [C₆H₆N⁺], 65 (31) [C₃H₅⁺]; elemental analysis calcd (%) for C₁₂H₁₂N₂S (216.30): C 66.63, H 5.59, N 12.95; found: C 66.72, H 5.81, N 13.05.

[FeL1(bpms)] (1a). A solution of [FeL1(MeOH)₂] (0.43 g, 0.85 mmol) and bpms (0.92 g, 4.25 mmol) in ethanol (50 mL) was heated to reflux for 4 h. After cooling to room temperature the fine crystalline black precipitate of **1a** formed within 24 h, which was filtered off, washed with ethanol (2 × 5 mL) and dried *in vacuo* (yield 0.42 g, 75%). IR (KBr): $\tilde{\nu}$ = 1676(*vs*) (COO), 1564(*vs*) cm⁻¹ (CO); MS (DEI(+), 70 eV): *m/z* (%): 443 (32) [FeL1⁺ + H], 442 (100) [FeL1⁺], 397 (28), 354 (30), 309 (28), 216 (15) [bpms⁺]; MS (ESI): *m/z* (%): 874 (9) [M⁺ + bpms], 658 (23) [M⁺], 442 (15) [FeL1⁺], 217 (100) [bpms⁺ + H]; elemental analysis calcd (%) for C₃₂H₃₄FeN₄O₆S (658.55): C 58.36, H 5.20, N 8.51; found: C 58.35, H 5.25, N 8.50. Crystals of **1a** were obtained by slow diffusion between a solution of [FeL1(MeOH)₂] (0.18 g, 0.35 mmol) in ethanol (15 mL) and a solution of bpms (0.08 g, 0.39 mmol) in ethanol (15 mL). After two weeks **1a** was obtained as black crystals.

[FeL1(bpms)] (1b). A solution of [FeL1(MeOH)₂] (0.42 g, 0.83 mmol) and bpms (1.55 g, 6.94 mmol) in methanol (30 mL) was heated to reflux for 1 h. After cooling to room temperature **1b** precipitated as a black, fine crystalline solid within 24 h, which was filtered off, washed with methanol (2 × 5 mL) and dried *in vacuo* (yield 0.27 g, 49%). Elemental analysis calcd (%) for C₃₂H₃₄FeN₄O₆S (658.55): C 58.36, H 5.20, N 8.51; found: C 58.26, H 5.29, N 8.50.

[FeL2(bpms)]·EtOH (2a·EtOH). A solution of [FeL2(MeOH)₂] (0.33 g, 0.86 mmol) and bpms (0.93 g, 4.32 mmol) in ethanol (50 mL) was heated to reflux for 4 h. After cooling to room temperature black crystals of **2a·EtOH** formed within 24 h, which were filtered off, washed with ethanol (2 × 5 mL) and dried *in vacuo* (yield 0.20 g, 36%). IR (KBr): $\tilde{\nu}$ = 1636(*vs*) (CO), 1559(*vs*) cm⁻¹ (CO); MS (DEI(+), 70 eV): *m/z* (%): 382 (99) [FeL2⁺], 367 (41), 340 (23), 354 (30), 216 (49) [bpms⁺], 93 (100); MS (ESI): *m/z* (%): 814 (5) [M⁺ + bpms], 581 (10) [M⁺], 423 (65), 382 (40) [FeL2⁺], 217 (100) [bpms⁺ + H]; elemental analysis calcd (%) for C₃₂H₃₆FeN₄O₅S (644.56): C 59.63, H 5.63, N 8.69; found: C 59.53, H 5.34, N 8.97.

[FeL2(bpms)]·MeOH (2b·MeOH). A solution of [FeL2(MeOH)₂] (0.28 g, 0.63 mmol) and bpms (0.68 g, 3.14 mmol) in methanol (17 mL) was heated to reflux for 1 h. After cooling to room temperature **2b·MeOH** precipitated immediately as black powder, which was filtered off, washed with methanol (2 × 5 mL) and dried *in vacuo* (yield 0.21 g, 53%). Elemental analysis calcd (%) for C₃₁H₃₄FeN₄O₅S (630.54): C 60.20, H 5.05, N 9.36; found: C 58.89, H 5.21, N 8.95.

[FeL3(bpms)] (3a). A solution of [FeL3(MeOH)₂] (0.24 g, 0.50 mmol) and bpms (0.54 g, 2.51 mmol) in ethanol (30 mL) was heated to reflux for 4 h. After cooling to room temperature a fine crystalline black precipitate of **3a** formed immediately, which was filtered off, washed with ethanol (2 × 5 mL) and dried *in vacuo* (yield 0.20 g, 63%). IR (KBr): $\tilde{\nu}$ = 1680(*vs*) (CO), 1566(*vs*) cm⁻¹ (CO); MS (DEI(+), 70 eV): *m/z* (%): 414 (100) [FeL3⁺], 383 (17), 340 (23), 309 (22), 216 (83) [bpms⁺], 93 (85); elemental analysis calcd (%) for C₃₀H₃₀FeN₄O₆S (630.49): C 57.15, H 4.80, N 8.89; found: C 57.04, H 4.86, N 8.86.

[FeL3(bpms)]·0.5MeOH (3b·0.5MeOH). A solution of [FeL3(MeOH)₂] (0.20 g, 0.61 mmol) and bpms (0.65 g, 3.00 mmol) in methanol (20 mL) was heated to reflux for 1 h. After cooling to room temperature **3b·0.5MeOH** precipitated immediately as a black, fine crystalline solid, which was filtered off, washed with methanol (2 × 5 mL) and dried *in vacuo* (yield 0.25 g, 66%). Elemental analysis calcd (%) for C_{30.5}H₃₂FeN₄O_{6.5}S (646.52): C 56.66, H 4.99, N 8.67; found: C 56.13, H 4.81, N 8.71.

[FeL4(bpms)] (4a). A solution of [FeL4(MeOH)₂] (0.19 g, 0.30 mmol) and bpms (0.33 g, 1.51 mmol) in ethanol (30 mL) was heated to reflux for 4 h. After cooling to room temperature a fine crystalline black precipitate of **4a** formed immediately, which was filtered off, washed with ethanol (2 × 5 mL) and dried *in vacuo* (yield 0.18 g, 77%). IR (KBr): $\tilde{\nu}$ = 1678(*s*) (CO), 1554(*s*) cm⁻¹ (CO); MS (DEI(+), 70 eV): *m/z* (%): 566 (100) [FeL3⁺], 521 (17), 369 (16), 216 (33) [bpms⁺], 93 (41); elemental analysis calcd (%) for C₄₂H₃₈FeN₄O₆S (782.68): C 64.45, H 4.89, N 7.16; found: C 64.19, H 5.00, N 7.17.

[FeL4(bpms)] (4b). A solution of [FeL4(MeOH)₂] (0.13 g, 0.21 mmol) and bpms (0.24 g, 1.00 mmol) in methanol (20 mL) was heated to reflux for 1 h. After cooling to room temperature **4b** precipitated immediately as black powder, which was filtered off, washed with methanol (2 × 5 mL) and dried *in vacuo* (yield 0.15 g, 90%). Elemental analysis calcd (%) for C₄₂H₃₈FeN₄O₆S (782.68): C 64.45, H 4.89, N 7.16; found: C 63.91, H 4.85, N 7.08. Crystals of **4b** were obtained by slow diffusion between a solution of [FeL4(MeOH)₂] (0.07 g, 0.11 mmol) in methanol (15 mL) and a solution of bpms (0.13 g, 0.60 mmol) in methanol (15 mL). After one week **4b** was obtained as black crystals.

Measurements

Magnetic susceptibility data were collected using a Quantum Design MPMSR-2 SQUID magnetometer under an applied field of 0.5 T over the temperature range 10–300 K and 10–350 K for **1b**. The samples were placed in gelatin capsules held within a plastic straw. The data were corrected for the diamagnetisation of the ligands, using tabulated Pascal's constants, and of the sample holder.

Differential scanning calorimetry (DSC) measurements were carried out in a He(g) atmosphere using a Perkin-Elmer DSC Pyris 1 instrument equipped with a cryostat and operating down to 98 K following a described procedure.²⁶

Single crystal X-ray structure determinations

The intensity data of **1a** and **4b** were collected on an Oxford XCalibur diffractometer using graphite-monochromated MoK_α

Table 5 Crystallographic data of the iron(II) complexes discussed in this work

Compound	1a	4b ^{HS}	4b ^{LS}
Formula	C ₃₂ H ₃₄ FeN ₄ O ₆ S	C ₄₂ H ₃₈ FeN ₄ O ₆ S	C ₄₂ H ₃₈ FeN ₄ O ₆ S
CCDC	729769	845684	845683
<i>M_r</i> /g mol ⁻¹	658.54	782.67	782.67
<i>S</i>	2	2	0
<i>λ</i> /Å	0.70930	0.70930	0.70930
<i>T</i> /K	225	250	125
Crystal system	Monoclinic	Orthorhombic	Orthorhombic
Space group	<i>P</i> 2 ₁ / <i>c</i>	<i>P</i> bca	<i>P</i> bca
<i>a</i> /Å	12.164(7)	19.2017(5)	18.8103(9)
<i>b</i> /Å	19.0805(11)	16.2729(8)	16.0825(7)
<i>c</i> /Å	16.115(7)	25.7799(15)	25.3728(13)
<i>α</i> /°	90.00	90	90
<i>β</i> /°	125.95(3)	90	90
<i>γ</i> /°	90.00	90	90
<i>V</i> /Å ³	3028(2)	8055.4(6)	7675.7(6)
<i>Z</i>	4	8	8
<i>ρ</i> _{calcd} /mg m ⁻³	1.445	1.291	1.355
<i>μ</i> /mm ⁻¹	0.619	0.477	0.501
<i>θ</i> range/°	3.78–26.31	4.24–26.27	4.22–26.27
Reflections collected	57 671	32 198	21 310
Indep. reflections (<i>R</i> _{int})	6157 (0.0604)	8144 (0.0376)	7753 (0.0292)
<i>R</i> (<i>F</i>) ^a (all data)	0.0363 (0.0571)	0.0346 (0.0815)	0.0324 (0.0625)
<i>wR</i> (<i>F</i> ²) ^b (all data)	0.0903 (0.1097)	0.0741 (0.0815)	0.0723 (0.0771)
GOF	1.064	0.823	0.878

^a $R(F) = \sum ||F_o| - |F_c|| / \sum |F_o|$; ^b $wR(F^2) = [\sum [w(F_o^2 - F_c^2)]^2 / \sum w(F_o^2)]^{1/2}$, $w = 1/[\sigma^2(F_o^2) + (aP)^2 + bP]$, where $P = [F_o^2 + 2(F_c^2)]/3$.

radiation. The data were corrected for Lorentz and polarisation effects. The structure was solved by Direct Methods (SIR 97)²⁷ and refined by full-matrix least-square techniques against *F*₀² (SHELXL-97).²⁸ The hydrogen atoms were included at calculated positions with fixed displacement parameters. ORTEP-III was used for structure representation,²⁹ SCHAKAL-99 to illustrate molecule packings.³⁰ The crystallographic data are summarised in Table 5.

Acknowledgements

The main part of the experiments was done at the University of Munich whose support is gratefully acknowledged. Support from the University of Bayreuth, the Deutsche Forschungsgemeinschaft (WE 3546_4-1), the Fonds der Chemischen Industrie, the IAP-VI (P6/17) INANOMAT, FNRS (FRFC 2.4.508.08 and IISN 4.4507.10) and ARC-Académie Louvain is gratefully acknowledged.

Notes and references

- (a) H. A. Goodwin, *Coord. Chem. Rev.*, 1976, **18**, 293; (b) E. König, *Struct. Bonding*, 1991, **76**, 51; (c) P. Gülich, A. Hauser and H. Spiering, *Angew. Chem., Int. Ed. Engl.*, 1994, **33**, 2024, and references therein; (d) Spin Crossover in Transition Metal Compounds I–III, in *Topics in Current Chemistry*, ed. P. Gülich and H. A. Goodwin, Springer-Verlag Berlin Heidelberg, New York, 2004; (e) J. A. Real, A. B. Gaspar and M. C. Muñoz, *Dalton Trans.*, 2005, 2062; (f) K. Nakano, N. Suemura, K. Yoneda, S. Kawata and S. Kaizaki, *Dalton Trans.*, 2005, 740; (g) O. Sato, J. Tao and Y.-Z. Zhang, *Angew. Chem.*, 2007, **119**, 2200; *Angew. Chem., Int. Ed.*, 2007, **46**, 2152; (h) J. A. Kitchen

- and S. Brooker, *Coord. Chem. Rev.*, 2008, **252**, 2072; (i) K. S. Murray, *Eur. J. Inorg. Chem.*, 2008, 3101; (j) M. A. Halcrow, *Coord. Chem. Rev.*, 2009, 2059; (k) S. Brooker and J. A. Kitchen, *Dalton Trans.*, 2009, 7331; (l) C. J. Kepert, *Aust. J. Chem.*, 2009, **62**, 1079; (m) K. S. Murray, *Aust. J. Chem.*, 2009, **62**, 1081; (n) A. B. Koudriavtsev and W. Linert, *J. Struct. Chem.*, 2010, **51**, 335.
- (a) O. Kahn and C. Jay Martinez, *Science*, 1998, **279**, 44; (b) O. Kahn, C. Jay, J. Kröber, R. Claude and F. Grolrière, *Pat.*, EP0666561, 1995; (c) J.-F. Létard, O. Nguyen and N. Daro, *Pat.*, FR0512476, 2005; (d) J.-F. Létard, P. Guionneau and L. Goux-Capes, *Topics in Current Chemistry*, ed. P. Gülich and H. A. Goodwin, Springer Wien New York, 2004, vol. 235, p. 221; (e) A. Galet, A. B. Gaspar, M. C. Muñoz, G. V. Bukin, G. Levchenko and J. A. Real, *Adv. Mater.*, 2005, **17**, 2949.
- Y. Garcia, V. Ksenofontov and P. Gülich, *Hyperfine Interact.*, 2002, **139/140**, 543.
- Y. Garcia, V. Ksenofontov, S. Mentior, M. M. Dirtu, C. Gieck, A. Bhatthacharjee and P. Gülich, *Chem.–Eur. J.*, 2008, **14**, 3745.
- Y. Garcia, V. Niel, M. C. Muñoz and J. A. Real, *Top. Curr. Chem.*, 2004, **233**, 195.
- J. A. Real, A. B. Gaspar, V. Niel and M. C. Muñoz, *Coord. Chem. Rev.*, 2003, **236**, 121.
- (a) B. Weber, *Coord. Chem. Rev.*, 2009, **253**, 2432–2449; (b) B. Weber and E.-G. Jäger, *Eur. J. Inorg. Chem.*, 2009, 465.
- (a) B. Weber, W. Bauer and J. Obel, *Angew. Chem., Int. Ed.*, 2008, **47**, 10098; (b) B. Weber, W. Bauer, T. Pfaffeneder, M. M. Dirtu, A. D. Naik, A. Rotaru and Y. Garcia, *Eur. J. Inorg. Chem.*, 2011, 3193–3206.
- (a) J.-F. Létard, P. Guionneau, E. Codjovi, O. Lavastre, G. Bravic, D. Chasseau and O. Kahn, *J. Am. Chem. Soc.*, 1997, **119**, 10861–10862; (b) Z. J. Zhong, J.-Q. Tao, Z. Yu, C.-Y. Dun, Y.-J. Lui and X.-Z. You, *J. Chem. Soc., Dalton Trans.*, 1998, 327–328.
- T. M. Pfaffeneder, S. Thallmair, W. Bauer and B. Weber, *New J. Chem.*, 2011, **35**, 691.
- W. Bauer, W. Scherer, S. Altmannshofer and B. Weber, *Eur. J. Inorg. Chem.*, 2011, 3183.
- G. S. Matouzenko, M. Perrin, B. le Guennic, C. Genre, G. Molnar, A. Bousseksou and S. A. Borshch, *Dalton Trans.*, 2007, 934.
- (a) G. S. Matouzenko, G. Molnar, N. Brefuel, M. Perrin, A. Bousseksou and S. A. Borshch, *Chem. Mater.*, 2003, **15**, 550; (b) C. Genre, G. S. Matouzenko, E. Jeanneau and D. Luneau, *New J. Chem.*, 2006, **30**, 1669; (c) B. Weber, R. Tandon and D. Himsl, *Z. Anorg. Allg. Chem.*, 2007, **633**, 1159; (d) B. Weber, E. S. Kaps, C. Desplanches and J.-F. Létard, *Eur. J. Inorg. Chem.*, 2008, 2963; (e) G. Dupouy, S. Triki, M. Marchivie, N. Cosquer, C. J. Gómez-García, S. Pillier, E. E. Bendeif, C. Lecomte, S. Asthana and J. F. Létard, *Inorg. Chem.*, 2010, **49**, 9358.
- C. Genre, E. Jeanneau, A. Bousseksou, D. Luneau, S. A. Borshch and G. S. Matouzenko, *Chem.–Eur. J.*, 2008, **14**, 697.
- J. Linares, H. Spiering and F. Varret, *Eur. Phys. J. B*, 1999, **10**, 271.
- S. M. Neville, B. A. Leita, G. J. Halder, C. Kepert, B. Moubaraki, J.-F. Létard and K. S. Murray, *Chem.–Eur. J.*, 2008, **14**, 10123.
- J. A. Rodriguez-Velamazán, M. Castro, E. Palacios, R. Burriel, T. Kitazawa and T. Kawasaki, *J. Phys. Chem. B*, 2007, **111**, 1256.
- B. Weber, E. Kaps, J. Weigand, C. Carbonera, J.-F. Létard, K. Achterhold and F.-G. Parak, *Inorg. Chem.*, 2008, **47**, 487.
- (a) T. Pfaffeneder, W. Bauer and B. Weber, *Z. Anorg. Allg. Chem.*, 2010, **636**, 183; (b) W. Bauer, T. Osslander and B. Weber, *Z. Naturforsch., B: J. Chem. Sci.*, 2010, **65**, 323.
- (a) A. B. Koudriavtsev, A. F. Strassen, J. G. Haasnoot, M. Grunert, P. Weinberger and W. Linert, *Phys. Chem. Chem. Phys.*, 2003, **5**, 3676; (b) A. B. Koudriavtsev, A. F. Strassen, J. G. Haasnoot, M. Grunert, P. Weinberger and W. Linert, *Phys. Chem. Chem. Phys.*, 2003, **5**, 3666.
- (a) C. A. Tovee, C. A. Kilner, J. A. Thomas and M. A. Halcrow, *CrystEngComm*, 2009, **11**, 2069; (b) Y. Shuku, R. Suizu, K. Awaga and O. Sato, *CrystEngComm*, 2009, **11**, 2065.
- Team of authors, *Organikum*, Johann Ambrosius Barth Leipzig, Berlin, Heidelberg, 1993.
- E.-G. Jäger, E. Häussler, M. Rudolph and M. Rost, *Z. Anorg. Allg. Chem.*, 1985, **525**, 67.

-
- 24 (a) B. Weber, H. Görls, M. Rudolf and E.-G. Jäger, *Inorg. Chim. Acta*, 2002, **337**, 247; (b) B. Weber, PhD thesis, University of Jena, 2002; Der Andere Verlag, Osnabrück, 2003.
- 25 B. Weber, R. Betz, W. Bauer and S. Schlamp, *Z. Anorg. Allg. Chem.*, 2010, **637**, 102.
- 26 A. Rotaru, M. M. Dirtu, C. Enachescu, R. Tanasa, J. Linares, A. Stancu and Y. Garcia, *Polyhedron*, 2009, **28**, 2531.
- 27 A. Altomare, M. C. Burla, G. M. Camalli, G. Cascarano, C. Giacovazzo, A. Guagliardi, A. G. G. Moliterni, G. Polidori and R. Spagna, *SIR-97*, University of Bari, Bari, Italy, 1997; *J. Appl. Crystallogr.*, 1999, **32**, 115.
- 28 G. M. Sheldrick, *SHELXL-97*, University of Göttingen, Göttingen, Germany, 1997.
- 29 C. K. Johnson and M. N. Burnett, *ORTEP-III*, Oak-Ridge National Laboratory, Oak-Ridge, TN, USA, 1996; L. J. Farrugia, *J. Appl. Crystallogr.*, 1997, **30**, 565.
- 30 E. Keller, *SCHAKAL-99*, University of Freiburg, Freiburg, Germany, 1999.